Characterization of Water Vapor and Clouds During the Next-Generation Aircraft Remote Sensing for Validation (NARVAL) South Studies

Sabrina Schnitt, Emiliano Orlandi, Mario Mech, André Ehrlich, and Susanne Crewell, *Member, IEEE*

***Abstract*—Shallow trade wind clouds pose one of the largest uncertainties in climate models. Due to the difficulties in assessing these clouds with routine observations the next-generation aircraft remote-sensing for validation campaign with the German High Altitude and LOng range research aircraft (HALO) took place in December 2013. Here we take advantage of the synergy of the HALO active and passive microwave package as well as spectrally resolved solar radiation (SR) measured by HALO-SR to characterize shallow clouds in the Caribbean. Based on a cloud mask developed from HALO-SR, about 12 000 cloudy profiles within ~ 4100 individual clouds could be detected with about 70 % of them having a length of less than 2 km. Corresponding measurements with passive microwave measurements reveal that these small clouds also contain little water with 36% of the clouds showing a liquid water path (LWP) of less than $50\,\mathrm{g}\cdot\mathrm{m}^{-2}$. We show that these small and thin clouds are difficult to characterize with satellite observations by the special sensor microwave imager/sounder due to its coarse resolution. Moderate imaging spectroradiometer measurements are able to identify the smaller clouds but suffer in terms of LWP when clouds start precipitating, which is the case for about 7% of the clouds as detected by the airborne 35 GHz radar.**

***Index Terms*—Airborne active and passive microwaves, cloud remote sensing, satellite.**

I. Introduction

THE uncertainty in the climate sensitivity of clouds strongly limits the reliability of climate model simulations [1], [2]. Especially, shallow marine boundary layer cumuli [3] in the trade-wind-driven regions over the subtropical oceans have been identified as a major source of observed intermodel spreads.

Manuscript received June 29, 2016; revised November 2, 2016, January 13, 2017, and February 24, 2017; accepted March 14, 2017. Date of publication May 31, 2017; date of current version July 26, 2017. This work was supported by the Deutsche Forschungsgemeinschaft through Projects "WE 1900/21-1" and "CR-111/9-1." *(Corresponding author: Mario Mech).*

S. Schnitt, M. Mech, and S. Crewell are with the University of Cologne, Cologne 50923, Germany (e-mail: sabrina.schnitt@uni-koeln.de; mario.mech@uni-koeln.de; CREWELL@meteo.uni-koeln.de).

E. Orlandi is with the University of Cologne, Cologne 50923, Germany, and also with Radiometer Physics GmbH, Meckenheim 53340, Germany (e-mail: emiliano.orlandi@radiometer-physics.de).

A. Ehrlich is with the University of Leipzig, Leipzig 04109, Germany (e-mail: a.ehrlich@uni-leipzig.de).

Color versions of one or more of the figures in this paper are available online at http://ieeexplore.ieee.org.

Digital Object Identifier 10.1109/JSTARS.2017.2687943

Due to their coarse resolution, global climate models of 100 km or more, clouds are not resolved but need to be parametrized (e.g., [4]). Evaluations of products such as cloud fraction using satellite data, however, show a mismatch between modeled and observed conditions [5]. Especially over remote areas of the globe, such as over the oceans, observations mainly emerge from satellite observations [6]. The liquid water content is especially important as it determines the cloud radiative properties and the generation of precipitation. However, discrepancies in cloud liquid water path (LWP) derived from different satellite sensors are observed depending on cloud-fraction [7], or vertical cloud structure assumptions [8]. The differences between satellite sensor products, but also between satellite and modeling results, require more detailed observations.

Whereas marine cloud *in situ* or ship-based measurements are limited in their spatial scale representativeness, airborne observations based on synergetic remote-sensing measurements offer the potential to not only cover large spatial regimes, but also to observe small scenes with high resolution and flexibility [9], [10]. Field studies investigating trade-wind-driven environments such as the Rain in Shallow Cumulus over the Oceans (RICO) [11], or the later Cloud, Aerosol, Radiation, and tuRbulence in the trade wInd regime over BArbados (CARRIBA) [12] studies try to answer problems in the characterization of shallow cumuli seen in other studies: Do they rain, and if so, how much precipitation do they contain [13]? How large are cumulus clouds [14]? How variable are the distributions of cloud sizes and scenes [15]?

To address the questions lined out above with an extended high-resolution dataset, but also to evaluate the suitability of coincident satellite observations the Next-generation Aircraft Remote-sensing for Validation studies (NARVAL-South, [16]) was performed, during which the German High Altitude and LOng range research aircraft (HALO) [17] performed research flights over the subtropical ocean east of Barbados. The synergy of the HALO active and passive Microwave Package (HAMP) and the HALO solar radiation instrument (HALO-SR) operating jointly during this campaign will be exploited to characterize individual trade-wind clouds and their statistical behavior. Furthermore, we will investigate whether operational satellite instruments capture these clouds but also their environment in terms of integrated water vapor (IWV). Our key focus is on the LWP as it determines the radiative properties of clouds and precipitation development.

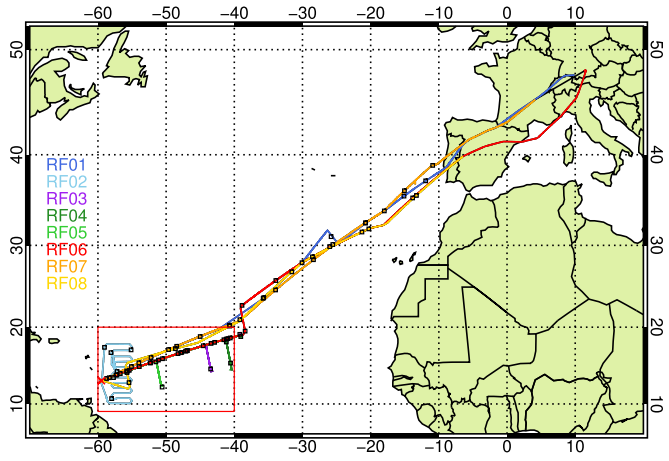

Fig. 1. NARVAL-South flight patterns with dropsonde launch positions marked in black and trade-wind-driven study region in red.

II. Observations

A. Airborne Measurements

The NARVAL-South campaign [16] was performed with the German HALO research aircraft in December 2013 encompassing four transfer flights between Oberpfaffenhofen, Germany, and Barbados as well as four local flights (see Fig. 1). Several underflights with the A-Train [18] were undertaken. A total of 68 flight hours on HALO took place from December 10–21, 2013, covering the meteorological situation in the dry winter season. With an average groundspeed of 234 m/s at flight altitudes averaging 13 km, HALO covered both trade-wind-dominated areas in the east of Barbados, as well as large-scale-driven patterns during transatlantic overpasses.

Standard *in situ* meteorology was measured by the BAsis HALO Measurement And Sensor System (BAHAMAS). In total 75 Vaisala dropsondes RD94 [19] provided *in situ* vertical profiles of temperature and humidity with 6–14 dropsondes launched per flight. Most importantly HALO was equipped with nadir-looking passive and active remote-sensing instruments mounted in a bellypod underneath the aircraft. All instruments were installed to be nadir pointing with a varying observation angle between 0° and 4° due to the aircraft pitch with slight differences in spatial and temporal resolution (see Table I). The footprint horizontal diameter of all instruments determined by their respective beamwidths is less than 1 km and reflects the instrument-specific lowest resolvable cloud length.

Nadir spectral solar radiance measurements covering the wavelength range 300–2200 nm were performed with the HALO-SR instrument [20]. The data were used to develop a cloud detection algorithm (cf. Section III-A). Furthermore, for some cases LWP, cloud droplet effective radius r_{eff} and optical depth τ has been derived using an iterative algorithm based on the radiance-ratio retrieval method developed by [21]. For NARVAL, due to a weak instrument sensitivity at wavelengths larger than 1500 nm, a radiance-ratio of 1050 and 1230 nm wavelength and the radiance at 870 nm were applied. The iterative algorithm successively adjusts LWP and r_{eff} until radiative transfer simulations agree with the HALO-SR measurements within predefined limits (0.005 for radiance-ratio and 0.005 $\text{Wm}^{-2}\text{sr}^{-1}\text{nm}^{-1}$ for radiance). Cloud optical depth was calculated using LWP and r_{eff} on basis of an adiabatic assumption [22]. In case of shallow cumuli, the adiabatic assumption may not be valid for all clouds leading to uncertainties in the retrieved cloud LWP. Similarly, the cloud inhomogeneities are not considered in the radiative transfer simulations. This simplification mostly increases the retrieval uncertainty in case of high solar zenith angles, when three-dimensional radiative effects (shadows and illuminated cloud sides) will dominate the radiative transfer.

The HAMP combines passive microwave radiometers with 26 channels between 22 and 200 GHz and a 35 GHz active cloud radar [9]. The increase in liquid water emission with frequencies allows a rather direct estimate of LWP from passive HAMP. Six channels along the wing of the 22.23 GHz H_2O line and two window channels (31.4 and 90 GHz) are used to simultaneously retrieve IWV and LWP using a statistical retrieval approach following [23] and [24]. In order to obtain a representative retrieval database, about 10 000 synthetic profiles were constructed from the combination of dropsonde thermodynamic profiles and low-level water clouds of different thickness and altitude. The clouds were chosen such that the retrieved LWP will be representative for the sum of cloud water and rain though strong rain events were not included. Radiative transfer calculations were performed to provide corresponding synthetic brightness temperatures to which normally distributed noise was added to mimic instrument accuracy. Due to the exclusion of strong rain events and given the frequencies used for the retrieval, scattering effect from rain droplets was not included in the radiative transfer simulations [23]. Retrieval coefficients were derived by applying a multivariable linear regression to the quadratic retrieval approach, including a term for sea-surface temperature (SST) [25] in order to account for the surface emission. Ocean emissivities were calculated using SST and satellite-derived 10 m wind speed [26]. The theoretical retrieval accuracy amounts to about 0.5 $\text{kg} \cdot \text{m}^{-2}$ for IWV and 28 $\text{g} \cdot \text{m}^{-2}$ for LWP. Note that, for the major part, the LWP uncertainty is caused by slowly varying components (drifts, changes in environmental conditions) rather than the sensitivity [24]. Due to the statistical retrieval approach, negative LWP values can occur. Therefore, special care is taken to improve the LWP estimate.

Because of the difficulties involved in the preflight radiometer calibration on the runway at Barbados airport, measured brightness temperatures were bias corrected based on the comparison with clear sky dropsondes. Radiative transfer calculations were performed for each sonde and, based on the mean offset, a constant for each research flight, and each frequency channel was determined. We follow the approach presented by van Meijgaard and Crewell [27] and made use of clear sky episodes (cf. Section III-A) to bias-correct the retrieved LWP. Each measurement's offset was calculated by forming a distance-weighted average LWP from all clear-sky cases within 30 min around each measurement. This clear-sky correction upscales 95% of all negative LWP values by on average 27.0 $\text{g} \cdot \text{m}^{-2}$ and shifts 1.3% into the positive value range. As we base our analyzes on the statistics of LWP rather than timeseries analysis, the remaining negative LWP values indicate the presence of statistical noise

TABLE I
INSTRUMENT CHARACTERISTICS OF AIRBORNE HAMP ACTIVE AND PASSIVE COMPONENT AND HALO-SR, AS WELL AS SPACEBORNE SSMIS AND MODIS

	Spectral range (number of channels)	Used frequencies	Across-track resolution	Temporal availability	Parameters
HAMP passive	22–200 GHz (26)	22.24, 23.04, 23.84, 25.44, 26.24, 27.84, 31.4, and 90 GHz	1 km * †	3 s	brightness temperature LWP IWV
HAMP active	35.5 GHz (1)	35.5 GHz	130 m *	1 s	equivalent reflectivity Z_e Doppler velocity
HALO-SR	300- 2200 nm (1056)	422, 532, 648, 858 1238, and 1638 nm	700 m *	1 s	spectral nadir radiance (I) effect. radius (r_{eff}), optical depth (τ), LWP
SSMIS	24–190 GHz (24)	19, 22.24, and 37 GHz	$0.25^\circ \times 0.25^\circ$	2 daily overpasses	IWV, LWP rain-rate, wind speed
AQUA MODIS	$0.4-14.4\,\mu$m (36)	0.66, 0.86, 1.2, 1.6 2.1 and 3.7 μm	1 km	2 daily overpasses	r_{eff}, τ, LWP

* at 13 km height † K-band channel

and are kept in order to avoid biases in the LWP distribution and average values (see [27] for further explanation).

The 35.5 GHz cloud radar measures profiles of the equivalent radar reflectivity factor Z_e. Its high sensitivity when operated on ground of -48 dBZ is reduced during airborne operation due to the contributions of the aircraft motion to the Doppler signal to about -30 dBZ when operated at 13 km [9]. Because the Z_e equals the sixth moment of the drop size distribution, the ability to detect thin low-level clouds without drizzle is limited.

The different instruments (see Table I) show different resolutions. In the following, the so-called D1 dataset considers measurements in the original spatial and temporal resolution of HAMP passive, HAMP active, and HALO-SR. These datasets are used for satellite evaluation and cloud length derivation. A merged dataset, called D2, has been generated containing valid data of all three instruments on the same time stamp. The D2 dataset is used in the following for analyzes based on the instrument synergy. All analyzes focus on a region between 9 and 20°N and -60 to -40°E where we assume the meteorological conditions to be driven by the trade winds.

B. Satellite Datasets

Global LWP climatologies rely on satellite observations over ocean with microwave imagers, i.e., the same principle as HAMP passive, considered to be the most reliable source [28], but suffer from rather coarse resolution of about 40 km. Near-infrared estimates by moderate imaging spectroradiometer (MODIS), based on the same principle as HALO-SR, have finer spatial resolutions but need to employ more assumptions [29].

The special sensor microwave imager (SSM/I) [30] and its successor the special sensor microwave imager and sounder (SSMIS) have been in orbit on various Defense Meteorological Satellite Program (DMSP) polar orbiting satellites since 1987. With their measurements in the microwave frequency range between 19.35 and 85.5 for SSM/I and 183.3 ± 6.6 for SSMIS, respectively, they are used to monitor hydrological parameters like water vapor and cloud water path and surface properties like sea ice coverage. Within this study, products derived from observations of the SSMIS sensor on the DMSP-F16 satellite provided by remote sensing systems [31] have been utilized to compare satellite- and airborne-derived water vapor and cloud characteristics. Thereby, IWV, LWP, wind speed, and rain-rate are retrieved from measurements at 19, 22.235, and 37 GHz and compiled to a product on a regular $0.25^\circ \times 0.25^\circ$ grid as described in [32], [33], and [28]. In case of rain, a cloud-rain partitioning threshold of LWP $= 180\,\mathrm{g \cdot m^{-2}}$ is applied, above which LWP is upscaled depending on the rain-rate. IWV is retrieved with a nominal accuracy of $1.2\,\mathrm{kg \cdot m^{-2}}$, whereas the lowest resolved LWP is $25\,\mathrm{g \cdot m^{-2}}$.

MODIS is operated on two near polar-orbiting satellite platforms, i.e., on Aqua within the A-train constellation [18] and on the Earth observing system satellite Terra. MODIS captures visible and near-infrared radiation in 36 channels with a horizontal across-track resolution of up to 250 m. Optical depth and effective radius is retrieved using reflectivity measurements and used to derive LWP [34]. A cloud mask algorithm uses several cloud detection tests to differentiate between clear and cloudy cases [35], [36]. We use the atmosphere level-2 product MYD06 with a spatial resolution of 1 km $\times$ 1 km available in collection 5.1, as well as the geolocation product MYD03 [37]. The data are filtered by applying quality flags, excluding cases where the retrieval failed, land impacted the view, or sun glint impacted the quality of the retrieval.

III. SYNERGY POTENTIAL

Similar as their space-borne counterparts HALO instruments show different sensitivities toward clouds. HALO-SR is most sensitive to thin water clouds due to their relatively high optical depth, HAMP passive relates most directly to LWP and the HAMP radar is strongly influenced by the presence of larger drops. The benefit resulting from their synergy is illustrated in the following.

A. Cloud Mask Algorithm

In order to distinguish between clear and cloudy cases, a cloud mask algorithm similar to the one deployed for MODIS

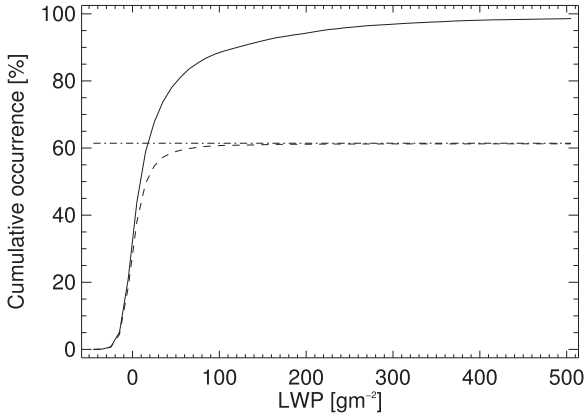

Fig. 2. Cumulative LWP distribution binned to $10\,\mathrm{g}\cdot\mathrm{m}^{-2}$ for all 12 224 cloudy flagged measurements (solid) and distribution for 7416 cases missed by the radar (dashed).

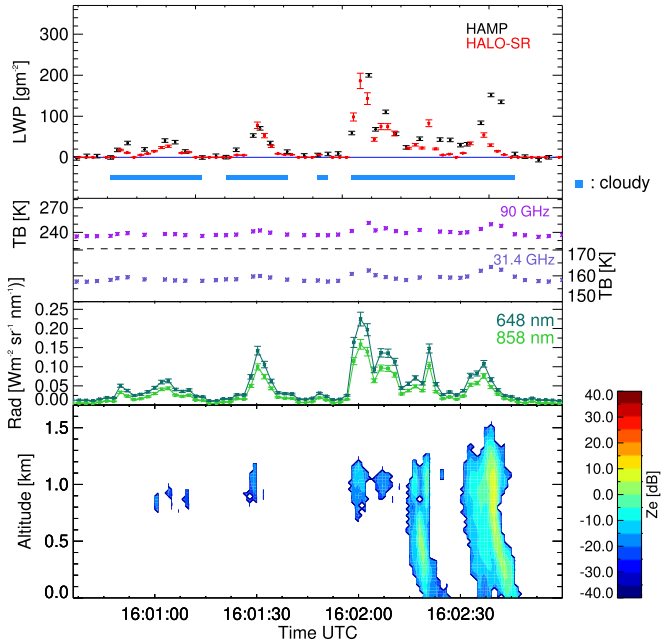

Fig. 3. Three min time series according to 34.7 km distance with LWP retrieved using HAMP and HALO-SR (top), 31.4 and 90 GHz brightness temperatures as well as 648 and 858 nm radiances (middle), 35 GHz radar backscatter reflectivity (bottom).

analysis was developed. It is based on nadir radiance I measured by HALO-SR at two wavelengths, $\lambda_1 = 648\,\mathrm{nm}$ and $\lambda_2 = 858\,\mathrm{nm}$. A measurement is attributed as "cloudy" if the ratio of $I(\lambda_2)$ and $I(\lambda_1)$, as well as the magnitude of one of the two radiance measurements exceed certain thresholds. We took advantage of the D2 radar reflectivities above 200 m and determined the thresholds by qualitatively comparing the distributions of $I(\lambda_1)$, $I(\lambda_2)$, and their ratio in clear and cloud-impacted cases. For the NARVAL observations, the thresholds were set to $\frac{I(\lambda_2)}{I(\lambda_1)} > 0.45$, $I(\lambda_1) > 0.01\,\mathrm{Wm^2sr^{-1}nm^{-1}}$, and $I(\lambda_2) > 0.008\,\mathrm{Wm^2sr^{-1}nm^{-1}}$. Comparing the number of cloudy cases determined by the cloud mask and by the radar, a cloud-mask hit-rate of 85.6% is reached.

B. Radar Performance

Based on the cloud mask performance, the radar signals of cloudy flagged cases were analyzed in order to quantify and characterize the amount of clouds missed by the radar due to sensitivity restrictions. For that purpose, the time-merged dataset D2 is used that contains the cloud flag, LWP, and the corresponding radar reflectivity profile. Considering all scenes identified as cloudy by the cloud mask, we find that in 60.7% of the cases no significant backscatter signal was detected by the radar. The reason for this lies in the dominance of rather thin clouds that is demonstrated by their median LWP of $5.9\,\mathrm{g}\cdot\mathrm{m}^{-2}$ (see Fig. 2). In 99% of the cases missed by the radar, LWP values do not reach $100\,\mathrm{g}\cdot\mathrm{m}^{-2}$. In the following, due to the sensitivity limit of the radar for the most frequent clouds, we only use the radar for precipitation detection because of its increased sensitivity to large drops and nonsaturation throughout the column.

C. LWP Retrieval Performance

In order to evaluate the LWP performance of the passive radiometer product, the retrieval noise was assessed using all scenes identified as clear by the cloud mask. As to be expected due to the offset correction applied (see Section II-A), the mean clear sky LWP is negligible with $\mu = -0.2\,\mathrm{g}\cdot\mathrm{m}^{-2}$. The LWP distribution is close to a Gaussian distribution with a standard deviation of $\sigma = 4.3\,\mathrm{g}\cdot\mathrm{m}^{-2}$. We neglect the occurring bias, and claim the standard deviation as sensitivity of the retrieval for further analyzes.

The relative performance of LWP retrieved by HAMP passive and by HALO-SR was compared for several case studies. A scene of coincident measurement from research flight RF03, December 13, 2013, is shown in Fig. 3. The radar data illustrate that the observed shallow cloud tops were located below 2 km altitude. Observations performed at the close-by Barbados Cloud Observatory [38] confirm that the cloud top heights match the height of the boundary layer inversion. In cases of nonprecipitating, shallow clouds as observed before 16:02 UTC, the LWPs retrieved from the two instruments agree within their uncertainties. However, if the clouds precipitate, as indicated by a high radar backscatter reflectivity ranging down to the ground as observed after 16:02:30 UTC, LWP from HAMP and HALO-SR disagree. HALO-SR significantly underestimates the amount of liquid with increasing precipitating amount compared to HAMP. These differences can be attributed to the different measurement techniques of the two instruments. The information content of the HALO-SR measurements mainly originates from cloud top since a major fraction of the reflected radiation is already scattered within the upper cloud layers, whereas HAMP is sensitive to the entire column. To derive LWP, the HALO-SR retrieval assumes an adiabatic cloud profile in the radiative transfer simulations of the retrieval algorithm. However, in case of drizzle or precipitation, droplet sizes may not follow the adiabatic assumption but rather increase nonhomogeneously with distance to cloud top. This leads to an underestimation of retrieved LWP in the HALO-SR retrieval as discussed by [39]. In order to

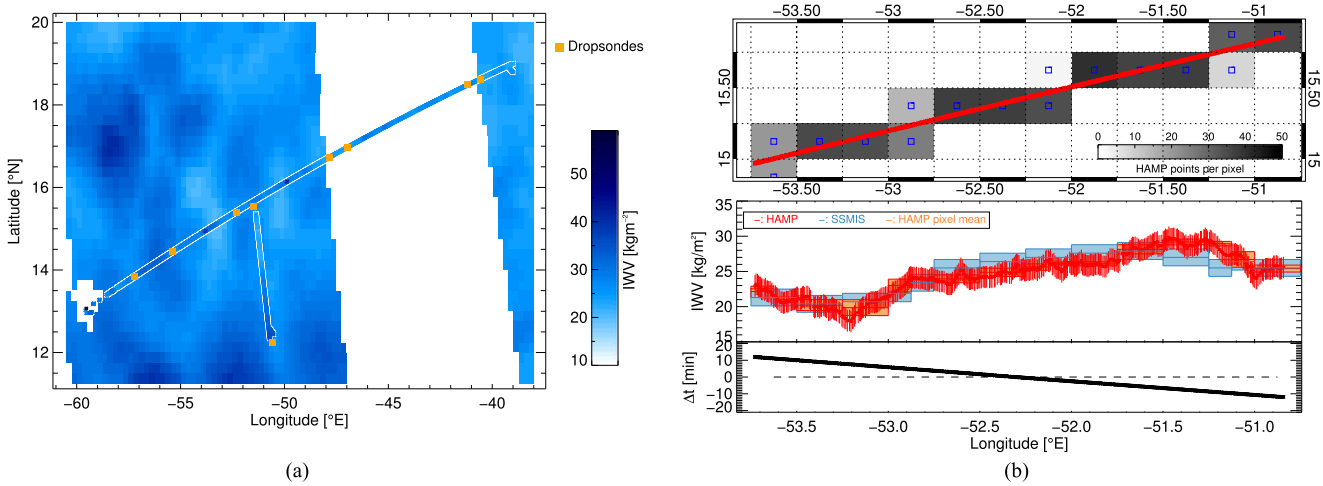

(a) (b)

Fig. 4. (a) IWV measured by SSMIS and HAMP during RF05. Dropsonde launch points are indicated in orange along the flight path. (b) Comparison of coincident IWV measurements during RF05. The upper panel shows the number of HAMP measurements per SSMIS pixel together with the HALO flight path (red). Flight direction is from right to left. The middle panel shows HAMP IWV with an uncertainty given by the dropsonde intercomparison (red), the mean HAMP value per SSMIS pixel (orange, box width represents measurements standard deviation per pixel), and SSMIS IWV with its uncertainty (blue). The bottom panel shows the time difference between HAMP and SSMIS measurements.

include thicker clouds in the following analyzes, the radiometer retrieved LWP product was chosen and analyzed statistically.

IV. Integrated Water Vapor

SSMIS water vapor observations are the most important source for long-term assessments of the water cycle and are frequently used to evaluate climate models (see for example [40]). The D1 dataset with HAMP IWV on a spatial resolution of about 1 km is used in the following analyzes to evaluate the coarser SSMIS IWV product on a grid of $0.25^\circ \times 0.25^\circ$.

In a first analysis, the two datasets are compared in a case study, taken from research flight RF05, December 15, 2013. On that day, HALO started from Barbados at 15:15 UTC, flying the same track east—as well as westwards on the return. The swath of the overpassing SSMIS evening orbit at 20:36 UTC (16:36 local time) shown in Fig. 4 reveals water vapor fields with variations on a scale of degrees in longitude and latitude. A positive North–South IWV gradient leads to increased IWV closer to the equator. The highly resolved HAMP IWV measurements, shown along the flight track throughout the entire flight, match the satellite measurements in most of the cases.

In the next step, a case study of direct pixel-by-pixel comparison of the differently resolved IWV products was performed, in which the same scene was observed by HAMP and SSMIS within 10 min. A 20 min. long case from research flight RF05, December 15, 2013 was selected to compare HAMP and SSMIS measurements [see Fig. 4(b)]. For each SSMIS pixel all HAMP IWV observations that occur within the pixel were averaged and compared to the satellite measurements. Differences can occur due to the time-shift between the measurements, or due to the fact that HAMP measurements are on a 11 km wide swath and cannot fully represent the intrapixel variability [10]. Encouragingly, the measurements agree well within the uncertainty of the SSMIS IWV and the standard deviation of HAMP IWV per pixel. The variability of IWV within each SSMIS pixel as assessed by HAMP does not exceed $1.3\,\mathrm{kg}\cdot\mathrm{m}^{-2}$, and therefore, does not limit the intercomparison significantly.

Expanding the case study approach to a comparison of all cases during the campaign in which HAMP and SSMIS captured the same scene within 1 h, 6288 HAMP measurements within 248 satellite pixels were compared as seen in Fig. 5. The amplitude of scatter around the 1:1-line does not show significant sensitivity to the time difference between the measurements. The negative bias between the two datasets of $-0.3\,\mathrm{kg}\cdot\mathrm{m}^{-2}$ shows a slight overestimation of the satellite IWV compared to the airborne data. The root mean squared difference (rms) of the two datasets is equal to $1.54\,\mathrm{kg}\cdot\mathrm{m}^{-2}$, comparable to the rms derived from a comparison between HAMP and dropsonde IWV ($1.53\,\mathrm{kg}\cdot\mathrm{m}^{-2}$). For the latter comparison, HAMP IWV was averaged over 30 s around each dropsonde launch and compared to the IWV derived by integrating the humidity along the descent of the dropsonde (see Fig. 4). Note, that the dropsonde relative humidity measurements have a nominal accuracy of 2%. The resulting bias of $-0.16\,\mathrm{kg}\cdot\mathrm{m}^{-2}$ also includes uncertainties due to horizontal drift of the dropsonde, as well as the (small) contribution of water vapor in the first 1 km below HALO, a region where the dropsonde measurements are discharged by the processing software. This similar rms shows that the coarsely resolved SSMIS product represents the water vapor variabilities as measured by fine-resolution air and *in situ* measurements. Therefore, given the uncertainty of the HAMP IWV retrieval, it is possible to conclude that SSMIS' spatial resolution is adequate to represent the water vapor variations, which in the region under exam mainly occur on scales larger than the satellite pixel.

V. Cloud LWP

A similar approach as used for IWV is performed to evaluate the LWP product of SSMIS using the HAMP D1 dataset. The same scene analyzed in Fig. 4 is shown in Fig. 6. Areas of

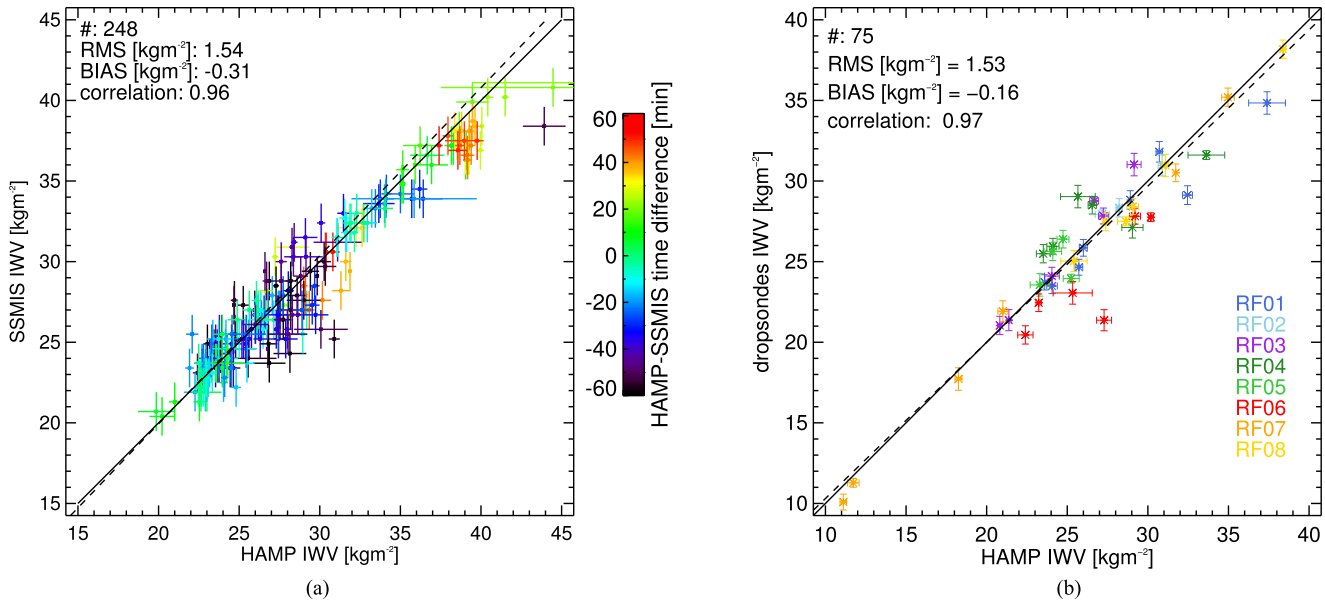

Fig. 5. IWV retrieved using HAMP in comparison with (a) coincident SSMIS measurements within 1 h time difference and (b) coincident dropsonde measurements. The x-values/x-error bars represent the mean/standard deviation of HAMP IWV (a) within each SSMIS pixel and (b) 30 s around each dropsonde launch. Colour scale indicates the time difference between HAMP and SSMIS measurements.

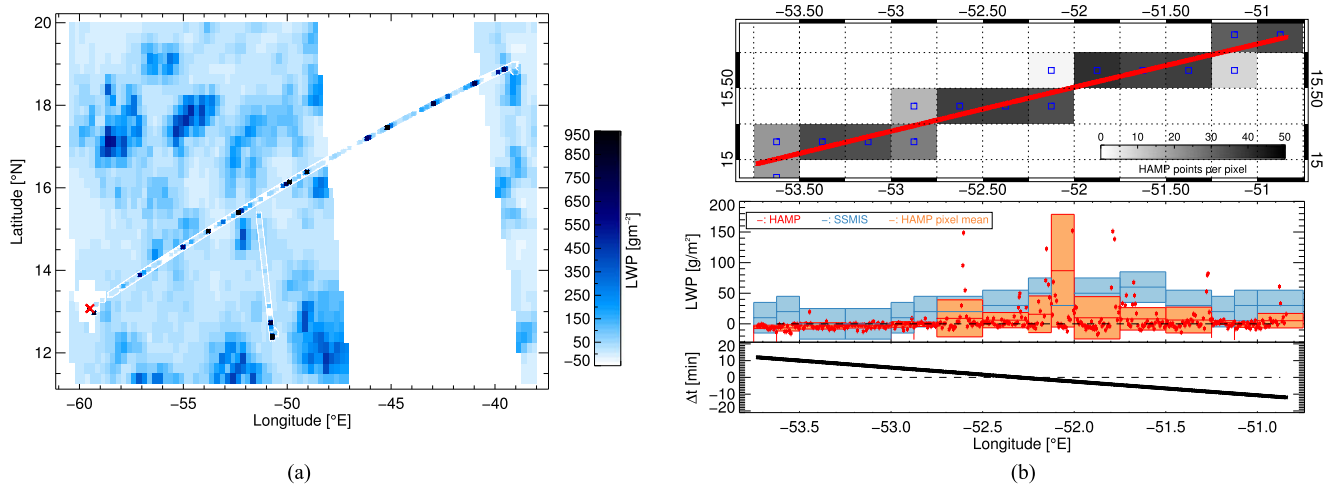

Fig. 6. (a) LWP measured by SSMIS during RF05 and by HAMP along the flight path. (b) As in Fig. 4 but for coincident LWP measurements.

heavy-loaded clouds with LWP larger than 500 g · m^{-2} match the areas of increased IWV. However, the spatial variability of LWP is much higher than for IWV with LWP significantly changing from pixel to pixel. A large variability is also found when analysing the highly resolved HAMP measurements on the spatial scale of a SSMIS pixel. This subpixel variability is confirmed when looking at the same period of coincident measurements of SSMIS and HAMP LWP as chosen before in the IWV case (see Fig. 6). Even though the SSMIS and HAMP pixel LWP values agree in 70% of the cases within their assigned uncertainties, the subpixel variability seen by HAMP reveals individual clouds with LWP up to 200 g · m^{-2} on a scale of less than 10 km, which are several times higher than the SSMIS pixel mean. These peaks not captured by SSMIS consist of only few HAMP measurements and are examples for the dominating shallow cumulus clouds regime in this area. As these clouds are small in size and cannot be captured by the SSMIS LWP, we conclude that SSMIS' coarse resolution is not sufficient to represent the LWP variability of the prevailing trade-wind cumuli. The nonuniform beamfilling becomes most problematic when pixels contain precipitating cells [41].

In a further approach, satellite data by Aqua MODIS with a spatial resolution of 1 km were analyzed for cases where the A-Train constellation overpassed HALO's flight track, as for example in research flight RF06, December 16, 2013, 16:00 - 16:15 UTC (see Fig. 7). The analysis was restricted to a period, in which both sensors captured the scene with less than 10 min of time difference. In this case, 41% of the MODIS data were

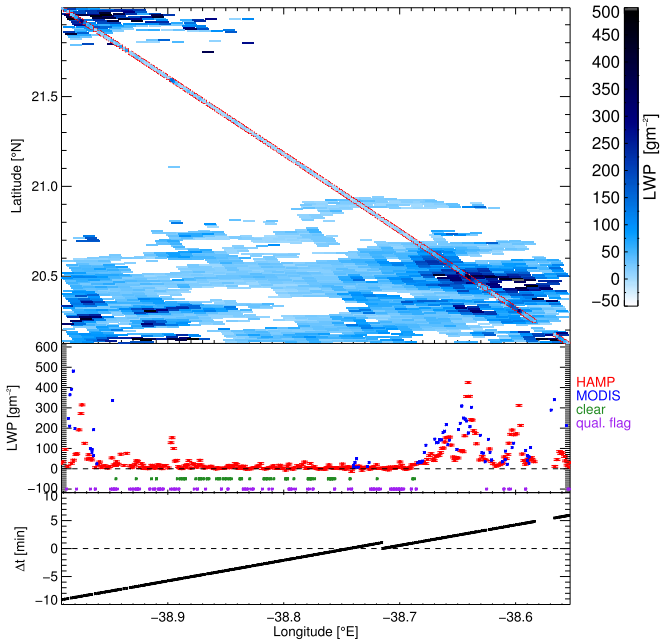

Fig. 7. Comparison of coincident LWP measurements by HAMP and MODIS during RF06 as a function of longitude. Shown are: the MODIS swath as well as HAMP LWP along the flight track, flight direction is from left to right (top panel); a direct comparison of LWP (HAMP in red, MODIS in blue), clear (green), and quality-flagged (purple) points (middle panel); the time difference between HAMP and MODIS measurements, with positive values representing a later MODIS measurement (bottom panel).

excluded due to poor quality flagging, and 27% of the measurements were marked as clear. In 56% of the cases where MODIS cloud-mask identified the scene as clear, the airborne measurements did not capture a cloud, either. In contrast to SSMIS, the small-scale variability of LWP is well captured by MODIS.

In cases where both sensors capture a cloud at the same position (around -38.6° E), MODIS underestimates the amount of LWP significantly for clouds with LWP higher than $200\,\mathrm{g}\cdot\mathrm{m}^{-2}$. HAMP measured LWP of 600 and $400\,\mathrm{g}\cdot\mathrm{m}^{-2}$, which are captured by MODIS with 350 and $120\,\mathrm{g}\cdot\mathrm{m}^{-2}$, respectively. This can either result from further cloud development within the 2 and 4 min of time difference between the measurements, but can also be caused by the differences in the two retrievals. Borg and Bennartz [8] found similar results by analysing stratiform marine boundary layer clouds with MODIS and AMSR-E LWP data. They find differences in LWP due to vertically homogeneous cloud structure assumed by the MODIS retrieval algorithm, leading to an underestimation of the real LWP. In contrast to their results, however, we find that in cases where HAMP captures clouds with LWP of less than $200\,\mathrm{g}\cdot\mathrm{m}^{-2}$, MODIS captures higher values as for example at -38.66° E. Zhou *et al.* [29] use microwave imager LWP estimates to improve the assumptions within the MODIS retrieval. However, within our study area, this approach might be difficult due to cloud variability.

The development of clouds on a time scale of several minutes is well visible in the peak around -39° E. HAMP and MODIS capture the same amount of LWP, but within the time between the two measurements, the cloud moved 0.01° further east. In cases around -38.9° E, HAMP captured cloud features, which are, however, not seen by MODIS. Within the 5 and 7 min of time difference, the clouds seem to have dissolved, as MODIS data are either flagged or marked as clear.

The intercomparison of HAMP LWP with the corresponding satellite estimates illustrated their limitations in terms of resolution and accuracy. In the following, we exploit HALO-SR and HAMP passive to assess shallow cloud properties.

VI. Cloud Properties

A. Cloud Length and LWP

When deriving the cloud lengths of the overflown single clouds, we focus on the temporally highest resolvable dataset D1 of HALO-SR. We base the analysis on the cloud mask performance and calculate cloud length as overflown distance between start and end point of each cloud. A cloud starts between the last clear and first cloudy measurement and ends between the last cloudy and first clear measurement to account for uncertainties at the cloud edges due to the data resolution (see Fig. 3 for illustration). Assuming 1-s time difference between subsequent measurements and a ground speed of 234 m/s, the smallest cloud length that can be calculated is 234 m. However, due to the footprint size of 700 m, the truly resolved cloud might be larger and lengths lower than the footprint size should be considered carefully. In total, we find 4165 trade-wind clouds with the calculation described above.

Fig. 8(a) shows the distribution of clouds that are smaller than 10 km, representing 93% of the D1 cloud population. The probability distribution $p(l)$ follows an exponential function of the form of $p(l) = al^{-\lambda}$, confirming the results of [14], [42], [43]. The distribution mean is located at 3.7 km, the median at 1 km. We find that 71% of the detected clouds are smaller than 2 km, 20% more than Zhao and Di Girolamo [14] who base their analyzes on a year-long dataset from a similar region using high spatially resolved data by the advanced spaceborne thermal emission and reflection radiometer. Differences between the results can arise due to the differences in the datasets in terms of time coverage and number of measurements, but also due to the sensitivity of our analysis to the cloud mask performance.

Next, we investigate how cloud length is related to the water content of the individual clouds. For that, we quantified the median cloud LWP by taking advantage of the HAMP passive measurements using the time-merged D2 dataset [see Fig. 8(b)]. Note that the number of detected clouds decreases to 2069 due to the lower time resolution of the dataset. Because of the higher temporal distance between measurement times, here the length of each cloud is calculated as distance between first and last cloudy flagged measurement adding one footprint length to account for the length calculation uncertainty. Due to the HALO-SR footprint size of 700 m (see Table I) and lower footprint overlap, no clouds smaller than ~500 m occurred. The distribution of cloud length occurrence follows a different exponential function than D1, as visible in Fig. 8(a). The artifacts in the small bins below 1.5 km are due to the high sensitivity of the length derivation to the resolution and processing of the data. Now, 55% of the clouds are classified smaller than 2 km in contrast to

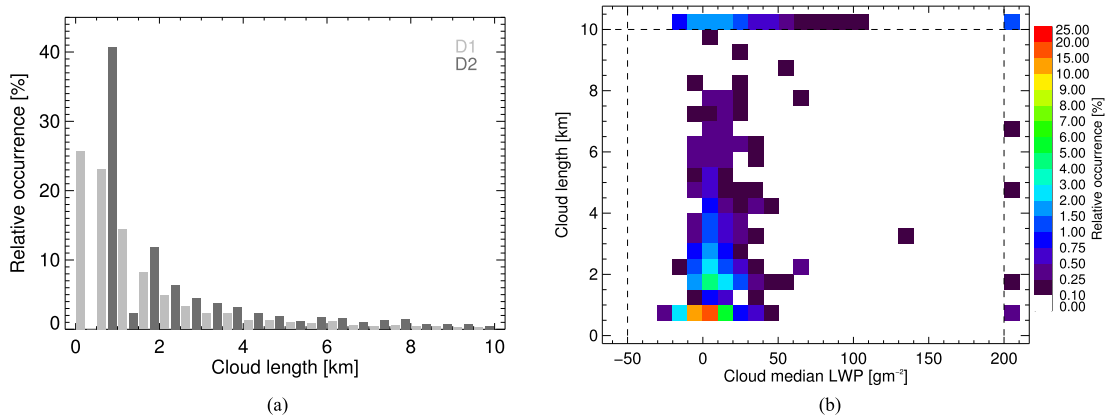

Fig. 8. (a) Cloud length probability distribution of 4165 trade-wind clouds (D1, light grey) and 2069 clouds (D2, dark grey) in 500 m bins and (b) 2D length and LWP distribution of 2069 clouds using the D2 dataset, binned to 500 m and 10 g · m^{-2}. Information beyond the dashed line represents all data beyond the respective limit.

the 71% in the original D1 resolution. This might be explained by the fact that small individual clouds are merged in the coarser resolution, indicating again the need for high-resolution measurements. The joint distribution of cloud median LWP and cloud length [see Fig. 8(b)] reveals that no linear relation between both exist. Small clouds containing rather low LWP, i.e., between 0–50 g · m^{-2} with lengths smaller than 2 km are evident 36% of the time. Interestingly, hardly any lengths larger than 8 km occur.

The limited predictability of cumulus-scale motions [44] make a direct comparison between simulated and observed cumulus clouds unfeasible. However, statistical approaches are used in order compare high-resolution simulations to experimental data, as for example performed during the RICO campaign (see [45]). Macrophysical and microphysical parameters, such as cloud length and LWP, respectively, determine radiative cloud properties, and are thus, important variables for cloud parametrization in models. By assessing these properties jointly rather than separately, more constraints can be put on the model in order to improve theoretical understanding. As illustrated by the difference of the D1 and D2 dataset, however, it is highly important that observations and model output are processed consistently.

B. Precipitating Clouds

The fraction of precipitating cloud is another interesting statistical relation that can be used to evaluate models and to investigate the autoconversion process. Several studies report different radar equivalent reflectivity thresholds to quantify the occurrence of precipitation [46]. Analyzes from the Barbados-located BCO [47] show signal-affection by precipitation from −20 dBZ on. We analyze the occurrence of precipitation based on the 35 GHz cloud radar in the merged D2 dataset. A profile is considered precipitating if the radar reflectivity close to the surface in the range bins between 50 and 200 m exceeds a threshold of −20 dBZ. Note, that due to shear effects and the time needed for drops to sediment no physical surface precipitation not necessarily is linked to the cloud above. We find that 7.4% of all considered profiles contain precipitation [see Fig. 9(a)]. Combining the presence of precipitation with the HAMP de-

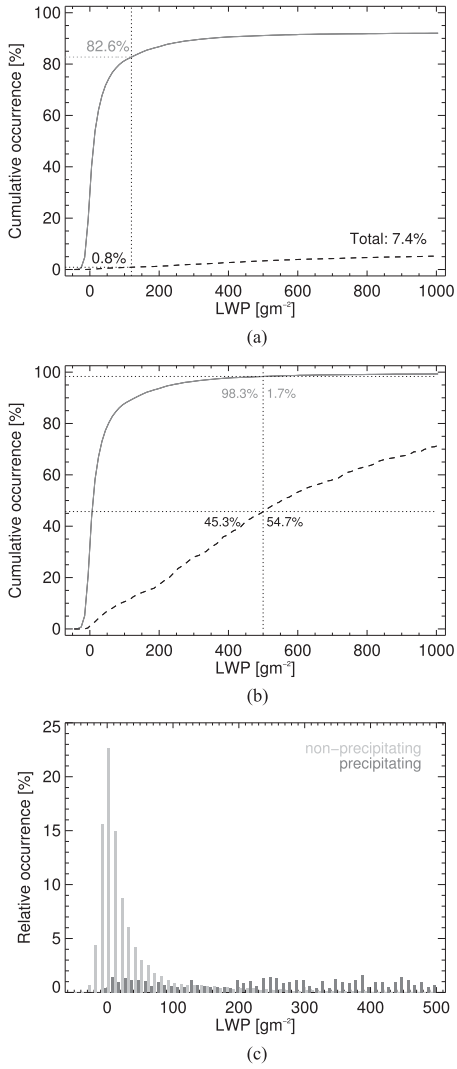

Fig. 9. (a), (b) Cumulative, and (c) normal LWP probability distribution for 967 precipitating (dark grey, dashed) and 12 224 nonprecipitating (light grey) cases, binned to 10 g · m^{-2}. (a) is normalized to the total number (13 191), (b) and (c) are normalized to the respective number of precipitating (967) and nonprecipitating (12 224) cases. The percentages given in (a) refer to the amount of data with LWP lower than 120 g · m^{-2}, in (b) to the amount of data smaller and greater than 500 g · m^{-2}.

rived LWP [see Fig. 9(a)], the cumulative occurrence of LWP increases monotonically in precipitating clouds, whereas LWP of nonprecipitating clouds starts saturating around 200 $g \cdot m^{-2}$ as most clouds contain very low LWP values (see Fig. 8). Cases of 500 $g \cdot m^{-2}$ and more occur with less than two percent in case of precipitation-free profiles, but with 54.7% for precipitating cases [see Fig. 9(b)]. Note, that 28.5% of the precipitating cases contain LWP higher than 1000 $g \cdot m^{-2}$ and lie beyond the range of the plot. 16.6% of all profiles contain 120 $g \cdot m^{-2}$ or more that can be derived by adding the cumulative precipitating (0.8%) and nonprecipitating (82.6%) occurrences in Fig. 9(a). As seen in Fig. 9(c), it is more likely that precipitation occurs in these cases.

These results can be used to evaluate the SSMIS cloud–rain partitioning LWP threshold of 180 $g \cdot m^{-2}$ reported by Wentz and Spencer [33]. Our results illustrate that there is no clear threshold but show that also clouds with lower LWP contain precipitation but with less likelihood. Because different factors such as the availability of cloud condensation nuclei contribute to the likelihood of precipitation, more studies for different climate zones and also other types as the shallow clouds studied here are needed.

VII. Conclusion

Shallow marine boundary layer clouds prevailing in the trade-wind-driven subtropical oceans constitute a major uncertainty in climate sensitivity studies. Intercomparison studies between different satellite sensors, also in comparison to model results, require product evaluation, for example by airborne campaigns. The NARVAL-South studies investigated shallow marine clouds driven by the trade winds over the North-Atlantic in December 2013. We combined three remote sensing instruments mounted on the research aircraft HALO to evaluate satellite products of LWP and IWV, and characterize the prevailing clouds as well as precipitation occurrence.

Based on solar radiance data measured by HALO-SR, a cloud mask algorithm was developed that allowed the detection of individual clouds and to improve the LWP estimate of HAMP using clear sky scenes leading to a sensitivity of better than 10 $g \cdot m^{-2}$. HAMP LWP that makes use of the direct emission of liquid water above the radiatively cold ocean (same principle as microwave imagers like SSMI/S) agrees well with independently retrieved LWP from HALO-SR in cases of shallow clouds. However, in cases of thicker clouds likely containing drizzle or precipitation particles, the HAMP retrievals disagree with HALO-SR underestimating the amount of liquid. This bias is attributed to assumptions on the cloud vertical composition applied in the near-infrared retrieval and agrees with similar retrieval uncertainties of satellite cloud retrieval, e.g., by MODIS, studied by [29].

The SSMIS IWV product resolved on a coarse $0.25^\circ \times 0.25^\circ$ grid showed large-scale variations on a scale of degrees in longitude and latitude. A comparison of the satellite measurements to the airborne HAMP IWV revealed a rms of 1.6 $kg \cdot m^{-2}$, similar to the rms derived from a comparison of HAMP and dropsonde derived IWV. We conclude that the satellite resolution is high enough to cover water vapor variabilities, in contrast to the LWP variations within each SSMIS pixel that are captured by high-resolution HAMP estimates.

Finer resolved MODIS data with a resolution of 1 km, analyzed in a case study, however, represent single trade-wind cumuli as seen from the aircraft. Direct comparisons of clouds coincidently measured by HAMP and MODIS show that MODIS underestimates the amount of LWP for clouds with more than 200 $g \cdot m^{-2}$, and overestimates the LWP for clouds with small LWP. As shown by other studies [8], these disagreements result from vertical homogeneity assumptions made in the LWP retrieval.

Based on the cloud mask, we find that 93% and 71% of the observed clouds in prevailing trade winds are smaller than 10 and 2 km, respectively. Former studies based on satellite data [14] only found 50% to be smaller than 2 km, which we explain with the differences in the datasets used and advocate the need for more detailed measurements in the future. About a third of these small clouds contain LWP less than 50 $g \cdot m^{-2}$. Using a simple radar reflectivity threshold of -20 dBZ close to the surface, we identified 7% of the clouds as precipitating. Precipitation not only occurred in cases of LWP larger than the cloud–rain partitioning threshold of 180 $g \cdot m^{-2}$ assumed by Wentz and Spencer [33] for SSMI retrievals, but also arose in shallower clouds.

Further studies will include the use of the cloud radar to investigate the formation of drizzle and to analyze the differences in the estimation of water content by microwave and near-infrared passive techniques as has been done for the satellite perspective by Lebsock and Su [48]. Ultimately, the data will be used to evaluate large Eddy simulations, which in a first assessment, showed high potential to improve current cloud parametrisation schemes. Observations of the follow-up campaign NARVAL-II, successfully performed in fall 2016, will expand the analyzes to the wet summer season, and will further deepen the understanding of clouds in the trade winds.

Acknowledgment

The authors particularly thank M. Hagen (DLR), L. Hirsch (MPI Hamburg), H. Konow (University of Hamburg), and M. Maahn (University of Cologne, now at NOAA) for their work on radar processing. Many more scientists, HALO pilots, and crew members were responsible for the success of the NARVAL research flights without whom this work would not have been possible.

References

[1] O. Boucher *et al.*, "Clouds and aerosols," in *Climate Change 2013: The Physical Science Basis. Contribution of Working Group I to the Fifth Assessment Report of the Intergovernmental Panel on Climate Change*. Cambridge, U.K.: Cambridge Univ. Press, 2013, pp. 571–657.

[2] J. Vial, J.-L. Dufresne, and S. Bony, "On the interpretation of inter-model spread in CMIP5 climate sensitivity estimates," *Climate Dyn.*, vol. 41, no. 11/12, pp. 3339–3362, 2013.

[3] S. Bony *et al.*, "Clouds, circulation and climate sensitivity," *Nature Geosci.*, vol. 8, no. 4, pp. 261–268, Apr. 2015.

[4] A. M. Tompkins, "A prognostic parameterization for the subgrid-scale variability of water vapor and clouds in large-scale models and its use to diagnose cloud cover," *J. Atmos. Sci.*, vol. 59, no. 12, pp. 1917–1942, 2002.

[5] H. Chepfer, S. Bony, D. Winker, M. Chiriaco, J.-L. Dufresne, and G. Sèze, "Use of CALIPSO lidar observations to evaluate the cloudiness simulated by a climate model," *Geophys. Res. Lett.*, vol. 35, no. 15, Aug. 2008, Art. no. L15704.
[6] G. L. Stephens and C. D. Kummerow, "The remote sensing of clouds and precipitation from space: A review," *J. Atmos. Sci.*, vol. 64, no. 11, pp. 3742–3765, Nov. 2007.
[7] Á. Horváth and C. Gentemann, "Cloud-fraction-dependent bias in satellite liquid water path retrievals of shallow, non-precipitating marine clouds," *Geophys. Res. Lett.*, vol. 34, no. 22, 2007, Art. no. L22806.
[8] L. A. Borg and R. Bennartz, "Vertical structure of stratiform marine boundary layer clouds and its impact on cloud albedo," *Geophys. Res. Lett.*, vol. 34, no. 5, 2007, Art. no. L05807.
[9] M. Mech *et al.*, "HAMP the microwave package on the High Altitude and LOng Range research aircraft (HALO)," *Atmos. Meas. Techn.*, vol. 7, no. 12, pp. 4539–4553, 2014.
[10] A. Lammert and F. Ament, "Capabilities and uncertainties of aircraft measurements for the validation of satellite precipitation productsa virtual case study," *Meteorologische Zeitschrift*, vol. 24, no. 5, pp. 495–502, 2015.
[11] R. M. Rauber *et al.*, "Rain in shallow cumulus over the ocean: The RICO campaign," *Bull. Amer. Meteorological Soc.*, vol. 88, pp. 1912–1928, 2007.
[12] H. Siebert *et al.*, "The fine-scale structure of the trade wind cumuli over Barbadosan introduction to the CARRIBA project," *Atmos. Chem. Phys.*, vol. 13, no. 19, pp. 10061–10077, 2013.
[13] L. Nuijens, B. Stevens, and A. P. Siebesma, "The environment of precipitating shallow cumulus convection," *J. Atmos. Sci.*, vol. 66, no. 7, pp. 1962–1979, July 2009.
[14] G. Zhao and L. Di Girolamo, "Statistics on the macrophysical properties of trade wind cumuli over the tropical western Atlantic," *J. Geophys. Res.*, vol. 112, no. D10, May 2007, Art. no. D10204.
[15] L. Nuijens, I. Serikov, L. Hirsch, K. Lonitz, and B. Stevens, "The distribution and variability of low-level cloud in the North Atlantic trades," *Quarterly J. Royal Meteorological Soc.*, vol. 140, no. 684, pp. 2364–2374, 2014.
[16] C. Klepp, F. Ament, S. Bakan, L. Hirsch, and B. Stevens, "NARVAL campaign report," Max-Planck-Inst. Meteorology, Hamburg, Germany, Tech. Rep. 164, 2014.
[17] H. Ziereis and M. Glässer, "Global Player für die Atmosphärenforschung - HALO," *DLR-Magazin*, vol. 115, pp. 3236, 2006.
[18] T. S. L'Ecuyer and J. H. Jiang, "Touring the atmosphere aboard the A-Train," *Phys. Today*, vol. 63, no. 7, pp. 36–41, 2010.
[19] T. F. Hock and J. L. Franklin, "The ncar GPS dropwindsonde," *Bull. Amer. Meteorological Soc.*, vol. 80, no. 3, pp. 407–420, 1999.
[20] C. Fricke, A. Ehrlich, E. Jäkel, B. Bohn, M. Wirth, and M. Wendisch, "Influence of local surface albedo variability and ice crystal shape on passive remote sensing of thin cirrus," *Atmos. Chem. Phys.*, vol. 14, no. 4, pp. 1943–1958, Feb. 2014.
[21] F. Werner, H. Siebert, P. Pilewskie, T. Schmeissner, R. A. Shaw, and M. Wendisch, "New airborne retrieval approach for trade wind cumulus properties under overlying cirrus," *J. Geophys. Res.: Atmos.*, vol. 118, no. 9, pp. 3634–3649, 2013.
[22] R. Wood and D. L. Hartmann, "Spatial variability of liquid water path in marine low cloud: The importance of mesoscale cellular convection," *J. Climate*, vol. 19, no. 9, pp. 1748–1764, 2006.
[23] U. Löhnert and S. Crewell, "Accuracy of cloud liquid water path from ground-based microwave radiometry 1. Dependency on cloud model statistics," *Radio Sci.*, vol. 38, no. 3, 2003, Art. no. 8041.
[24] S. Crewell and U. Löhnert, "Accuracy of cloud liquid water path from ground-based microwave radiometry 2. Sensor accuracy and synergy," *Radio Sci.*, vol. 38, no. 3, 2003, Art. no. 8042.
[25] R. W. Reynolds, T. M. Smith, C. Liu, D. B. Chelton, K. S. Casey, and M. G. Schlax, "Daily high-resolution-blended analyses for sea surface temperature," *J. Climate*, vol. 20, no. 22, pp. 5473–5496, 2007.
[26] H.-M. Zhang, J. J. Bates, and R. W. Reynolds, "Assessment of composite global sampling: Sea surface wind speed," *Geophys. Res. Lett.*, vol. 33, no. 17, 2006, Art. no. L17714.
[27] E. van Meijgaard and S. Crewell, "Comparison of model predicted liquid water path with ground-based measurements during CLIWA-NET," *Atmos. Res.*, vol. 75, no. 3, pp. 201–226, 2005.
[28] C. W. O'Dell, F. J. Wentz, and R. Bennartz, "Cloud liquid water path from satellite-based passive microwave observations: A new climatology over the global oceans," *J. Climate*, vol. 21, no. 8, pp. 1721–1739, 2008.
[29] L. Zhou, Q. Liu, D. Liu, L. Xie, L. Qi, and X. Liu, "Validation of MODIS liquid water path for oceanic nonraining warm clouds: Implications on the vertical profile of cloud water content," *J. Geophys. Res.: Atmos.*, vol. 121, no. 9, pp. 4855–4876, 2016.
[30] J. P. Hollinger, "DMSP special sensor microwave/imager calibration/validation," Nav. Res. Lab., vol. 1, 1989.
[31] F. J. Wentz, K. Hilburn, and D. K. Smith, "RSS SSMIS ocean product grids daily from DMSP F16 NETCDF [indicate subset used]," Dataset available online from the NASA Global Hydrology Center DAAC, Huntsville, Alabama, U.S.A., 2012.
[32] F. J. Wentz, "A well-calibrated ocean algorithm for special sensor microwave/imager," *J. Geophys. Res.: Oceans*, vol. 102, no. C4, pp. 8703–8718, Apr. 1997.
[33] F. J. Wentz and R. W. Spencer, "SSM/I rain retrievals within a unified all-weather ocean algorithm," *J. Atmos. Sci.*, vol. 55, no. 9, pp. 1613–1627, 1998.
[34] S. Platnick *et al.*, "The MODIS cloud products: Algorithms and examples from Terra," *IEEE Trans. Geosci. Remote Sens.*, vol. 41, no. 2, pp. 459–473, Feb. 2003.
[35] S. A. Ackerman, K. I. Strabala, W. Paul Menzel, R. A. Frey, C. C. Moeller, and L. E. Gumley, "Discriminating clear sky from clouds with MODIS," *J. Geophys. Res.: Atmos.*, vol. 103, no. D24, pp. 32141–32157, 1998.
[36] R. A. Frey *et al.*, "Cloud detection with MODIS. Part I: Improvements in the MODIS cloud mask for collection 5," *J. Atmos. Oceanic Technol.*, vol. 25, no. 7, pp. 1057–1072, 2008.
[37] S. Platnick *et al.*, "MODIS atmosphere L2 cloud product (06_L2)," NASA MODIS Adaptive Processing System, Goddard Space Flight Center, 2015.
[38] B. Stevens *et al.*, "The barbados cloud observatory: Anchoring investigations of clouds and circulation on the edge of the ITCZ," *Bull. Amer. Meteorological Soc.*, vol. 97, no. 5, pp. 787–801, May 2016.
[39] D. J. Miller, Z. Zhang, A. S. Ackerman, S. Platnick, and B. A. Baum, "The impact of cloud vertical profile on liquid water path retrieval based on the bispectral method: A theoretical study based on large-eddy simulations of shallow marine boundary layer clouds," *J. Geophys. Res.: Atmos.*, vol. 121, no. 8, pp. 4122–4141, 2016.
[40] K. E. Trenberth, J. Fasullo, and L. Smith, "Trends and variability in column-integrated atmospheric water vapor," *Climate Dyn.*, vol. 24, no. 7/8, pp. 741–758, Mar. 2005.
[41] L. V. Bremen, E. Ruprecht, and A. Macke, "Errors in liquid water path retrieval arising from cloud inhomogeneities: The beam-filling effect," *Meteorologische Zeitschrift*, vol. 11, no. 1, pp. 13–19, Mar. 2002.
[42] R. A. J. Neggers, H. J. J. Jonker, and A. P. Siebesma, "Size statistics of cumulus cloud populations in large-eddy simulations," *J. Atmos. Sci.*, vol. 60, no. 8, pp. 1060–1074, Apr. 2003.
[43] R. Wood and P. R. Field, "The distribution of cloud horizontal sizes," *J. Climate*, vol. 24, no. 18, pp. 4800–4816, Sept. 2011.
[44] E. N. Lorenz, "The predictability of a flow which possesses many scales of motion," *Tellus*, vol. 21, no. 3, pp. 289–307, 1969.
[45] M. C. van Zanten *et al.*, "Controls on precipitation and cloudiness in simulations of trade-wind cumulus as observed during rico," *J. Adv. Model. Earth Syst.*, vol. 3, no. 2, 2011, Art. no. M06001.
[46] Y. Liu, B. Geerts, M. Miller, P. Daum, and R. McGraw, "Threshold radar reflectivity for drizzling clouds," *Geophys. Res. Lett.*, vol. 35, no. 3, Feb. 2008, Art. no. L03807.
[47] K. Lamer, P. Kollias, and L. Nuijens, "Observations of the variability of shallow trade wind cumulus cloudiness and mass flux," *J. Geophys. Res.: Atmos.*, vol. 120, no. 12, pp. 6161–6178, June 2015.
[48] M. Lebsock and H. Su, "Application of active spaceborne remote sensing for understanding biases between passive cloud water path retrievals," *J. Geophys. Res.: Atmos.*, vol. 119, no. 14, pp. 8962–8979, 2014.

Sabrina Schnitt received the B.Sc. degree in physics from Free University Berlin, Berlin, Germany, in 2013, the M.Sc. degree in physics from the University of Cologne, Cologne, Germany.

Her main research interests include cloud remote sensing and passive microwave radiometry.

Emiliano Orlandi received the M.S. degree in physics from the University of Milano, Milano, Italy, in 2005 and the Ph.D. degree in physics from the University of Ferrara, Ferrara, Italy, in 2010.

During 2010, he was in the Institute of Atmospheric Science and Climate of the National Research Council of Italy (ISAC-CNR) as a Research Scientist. From 2011 to 2016, he was a Research Scientist in the Institute for Geophysics and Meteorology, University of Cologne, Cologne, Germany. He is currently with the Remote Sensing Division of Radiometer Physics GmbH, Meckenheim, Germany. His principal research interest include atmospheric radiative transfer modeling and retrieval processes.

Mario Mech received the Ph.D. degree in meteorology from the University of Cologne, Cologne, Germany, in 2008.

He is working as a Research Scientist in the Institute for Geophysics and Meteorology, University of Cologne, Cologne, Germany. His research interests include the active and passive microwave remote sensing of clouds and precipitation from airborne and spacebased plattforms. He is working as well on the radiative transfer simulation of active and passive microwave radiation in cloudy and rainy atmospheres.

André Ehrlich received the Ph.D. degree in meteorology from the Johannes Gutenberg University, Mainz, Germany, in 2009.

Since 2009, he has been with the University Leipzig, Leipzig, Germany. His research interests include the radiative and microphysical properties of clouds and snow surfaces. He has worked on airborne remote sensing using spectral solar radiation measurements. He developed and applied retrieval algorithms for cloud and snow properties utilizing the spectral and directional information of the measured radiation field. In particular, his interest focuses on the Arctic environment.

Susanne Crewell (M'06) received the Ph.D. degree in physics from the University of Bremen, Bremen, Germany, in 1993 and the Habilitation degree in meteorology from the University of Bonn, Bonn, Germany, in 2002.

From 2004 to 2006, she was a Professor of experimental meteorology with the Ludwig Maximilians University, Munich, Germany. She is currently a Full Professor of meteorology with the University of Cologne, Cologne, Germany. Her research interests include active and passive microwave remote sensing of the Earth, with a focus on the water and energy cycle. She has worked on latent heat flux determination from satellite; observation of stratospheric trace gases from aircraft and ground; and tropospheric water vapor, temperature, and hydrometeors. Her main interests include the combination of observations in different spectral regions and the use of observations for improving numerical weather forecast and climate models.